2019

Bone marrow dendritic cells regulate hematopoietic stem/progenitor cell trafficking

Jingzhu Zhang

Teerawit Supakorndej

Joseph R. Krambs

Mahil Rao

Grazia Abou-Ezzi

See next page for additional authors

Authors

Jingzhu Zhang, Teerawit Supakorndej, Joseph R. Krambs, Mahil Rao, Grazia Abou-Ezzi, Rachel Y. Ye, Sidan Li, Kathryn Trinkaus, and Daniel C. Link

Bone marrow dendritic cells regulate hematopoietic stem/progenitor cell trafficking

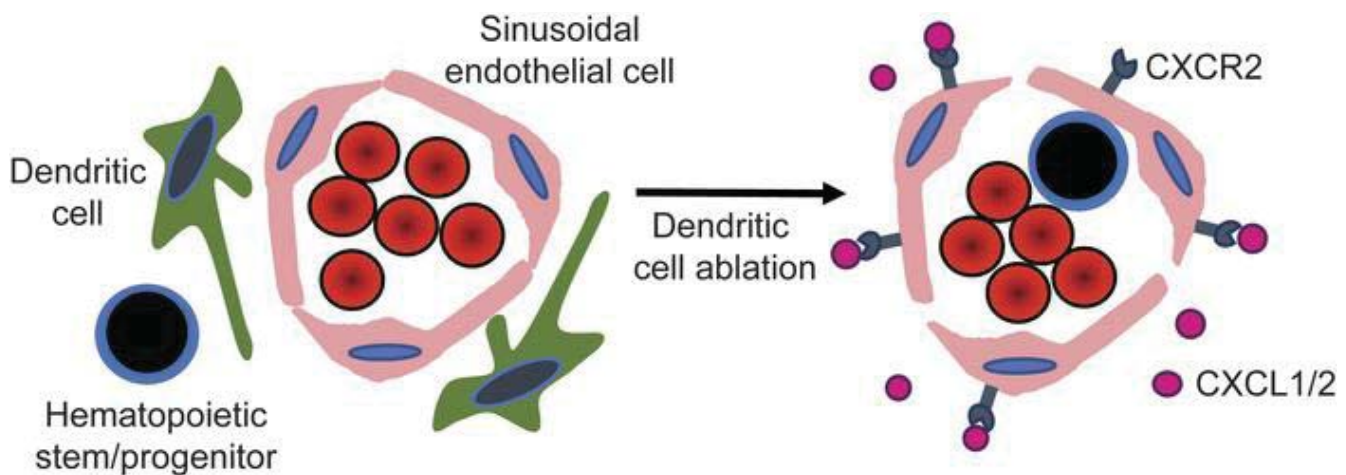Jingzhu Zhang, … , Kathryn Trinkaus, Daniel C. Link

Graphical abstract

Bone marrow dendritic cells regulate hematopoietic stem/progenitor cell trafficking

Jingzhu Zhang,[1] Teerawit Supakorndej,[1] Joseph R. Krambs,[1] Mahil Rao,[1] Grazia Abou-Ezzi,[1] Rachel Y. Ye,[1] Sidan Li,[1,2] Kathryn Trinkaus,[3] and Daniel C. Link[1]

[1]Division of Oncology, Department of Medicine, Washington University School of Medicine, Saint Louis, Missouri, USA. [2]Hematology Oncology Center, Beijing Children's Hospital, National Center for Children's Health, Capital Medical University, Beijing, China. [3]Biostatistics Shared Resource, Siteman Cancer Center, Washington University School of Medicine, Saint Louis, Missouri, USA.

A resident population of dendritic cells (DCs) has been identified in murine bone marrow, but its contribution to the regulation of hematopoiesis and establishment of the stem cell niche is largely unknown. Here, we show that murine bone marrow DCs are perivascular and have a type 2 conventional DC (cDC2) immunophenotype. RNA expression analysis of sorted bone marrow DCs showed that expression of many chemokines and chemokine receptors is distinct from that observed in splenic cDC2s, suggesting that bone marrow DCs might represent a unique DC population. A similar population of DCs was present in human bone marrow. Ablation of conventional DCs (cDCs) results in hematopoietic stem/progenitor cell (HSPC) mobilization that was greater than that seen with ablation of bone marrow macrophages, and cDC ablation also synergizes with granulocyte–colony stimulating factor to mobilize HSPCs. Ablation of cDCs was associated with an expansion of bone marrow endothelial cells and increased vascular permeability. CXCR2 expression in sinusoidal endothelial cells and the expression of 2 CXCR2 ligands, CXCL1 and CXCL2, in the bone marrow were markedly increased following cDC ablation. Treatment of endothelial cells in vitro with CXCL1 induced increased vascular permeability and HSPC transmigration. Finally, we showed that HSPC mobilization after cDC ablation is attenuated in mice lacking CXCR2 expression. Collectively, these data suggest that bone marrow DCs play an important role in regulating HSPC trafficking, in part, through regulation of sinusoidal CXCR2 signaling and vascular permeability.

Introduction

Under basal conditions, the majority of hematopoietic stem and progenitor cells (HSPCs) reside in specialized environments within the bone marrow termed the hematopoietic niche. The majority of hematopoietic stem cells (HSCs) are perivascular, where they are in close contact with endothelial cells and CXCL12-expressing mesenchymal stromal cells (1–4). HSPCs are mobilized into the circulation in response to a number of stimuli, including hematopoietic growth factors, myeloablative agents, and environmental stresses such as infection. Mobilized HSPCs have become the preferred cellular source for reconstitution of the bone marrow following myeloablative therapy because of their potency, predictability, and safety. Granulocyte–colony stimulating factor (G-CSF), a hematopoietic growth factor, is the mobilizing agent most commonly used in a clinical setting.

There is strong evidence that most mobilizing agents, including G-CSF, induce HSPC egress by altering the bone marrow microenvironment. HSPC mobilization by G-CSF is primarily mediated by suppressing CXCL12 expression in bone marrow mesenchymal stromal cells, the major ligand for CXCR4 (5–7). We previously showed that G-CSF signaling in monocytic cells in the bone marrow is sufficient to downregulate CXCL12 expression and induce robust HSPC mobilization (8). Consistent with this finding, 2 groups showed that ablation of bone marrow macrophages results in HSPC mobilization (9, 10). Together, these observations suggest that bone marrow macrophages play an important role in regulating HSPC trafficking from the bone marrow, although the signals that mediate this response are unknown.

Dendritic cells (DCs) are professional antigen presenting cells that are present in most tissues. In addition to antigen presentation, DCs contribute to immune cell activation through the secretion of cytokines and chemokines. DCs display considerable phenotypic and functional heterogeneity. DCs can be broadly classified, based on morphology, cell surface receptor expression, and developmental requirements, into 3 major groups: plasmacytoid DCs, type 1 conventional DCs (cDC1s), and type 2 conventional DCs (cDC2s). Expression profiles of conventional DCs (cDCs) vary significantly based on tissue type, suggesting that cDCs may play distinct roles in different tissue (11). Single-cell RNA sequencing suggests that there may be considerable heterogeneity of DCs even within a single tissue type. For example, single-cell RNA sequencing identified at least 4 discrete cDC populations in human blood (12).

Prior studies have identified a resident population of DCs in the bone marrow and provided evidence that these cells promote the survival of recirculating mature B cells and regulate memory T cells in the bone marrow (13, 14). Whether these cells regulate other aspects of hematopoiesis is currently unknown. In this study, we provide evidence that bone marrow DCs are a functionally distinct
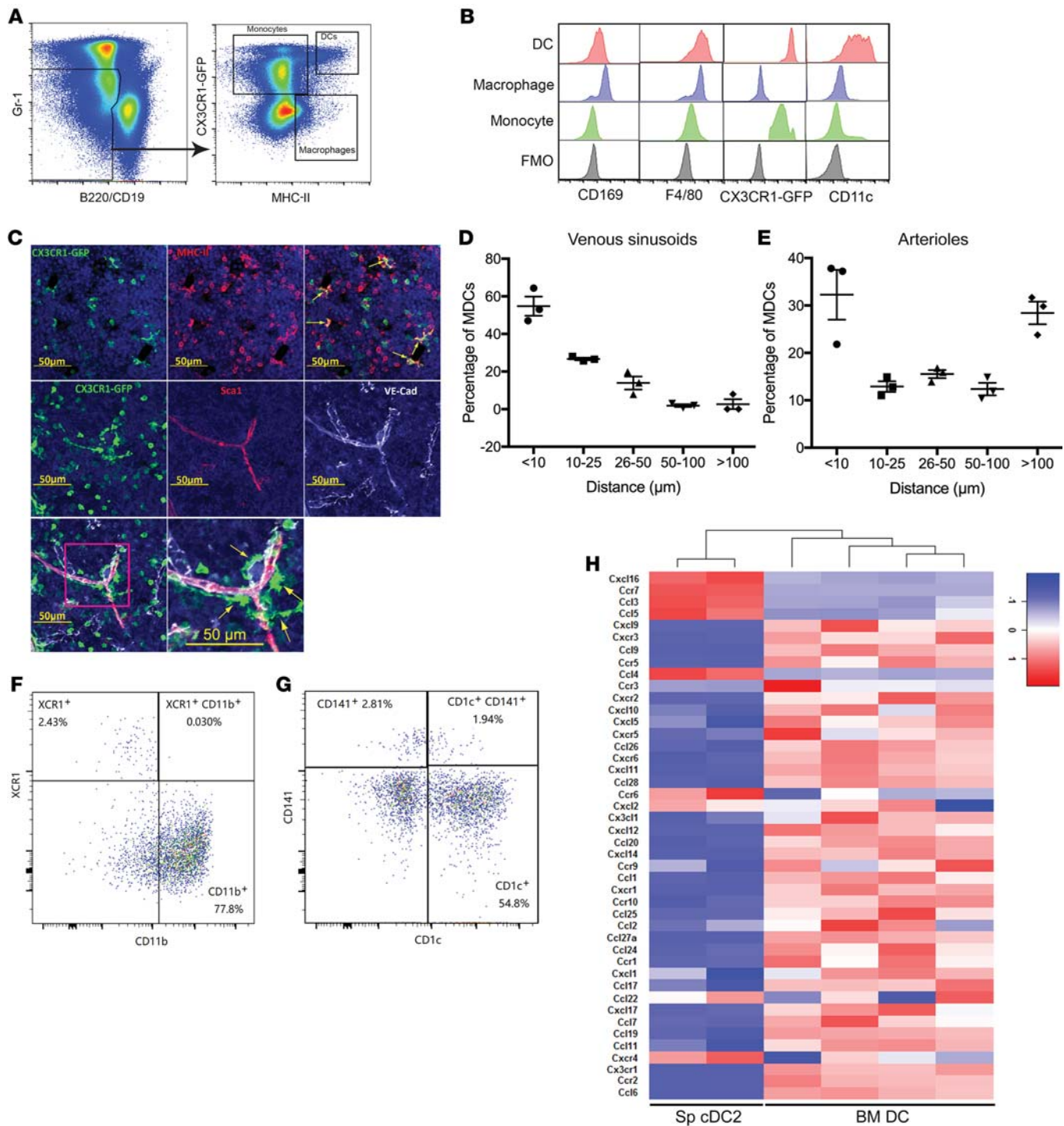
Figure 1. The majority of bone marrow dendritic cells have a cDC2-like phenotype, are enriched in the perivascular region, and have a unique RNA expression profile. (**A**) Representative flow plots showing the gating strategy used to identify bone marrow monocytes, macrophages, and DCs using *Cx3cr1CX*$^{gfp/+}$ mice. (**B**) The gated monocyte, macrophage, and DC populations were profiled for expression of the indicated lineage markers. FMO, fluorescence minus one control. (**C**) Representative photomicrographs of femur sections from *Cx3cr1*$^{gfp/+}$ mice. Top: CX3CR1-GFP (green) and MCH-II (red). Middle and bottom: CX3CR1-GFP (green), Sca1$^+$ arterioles (red), VE-cadherin$^+$ venous sinusoids and arterioles (white). Yellow arrows indicate DCs. Counterstaining with DAPI highlights nuclei (blue). (**D**, **E**) Quantification of the distance from DCs to the nearest venous sinusoid (**D**) or arteriole (**E**) (data pooled from *n* = 3 mice). (**F**) Representative flow plot showing expression of 2 murine cDC markers, XCR1 for cDC1 and CD11b for cDC2. Data are gated on Gr-1$^-$ B220$^-$ MHC-II^{hi} CD11c^{hi} DCs. (**G**) Representative flow plot showing the expression of 2 human cDC markers, CD141 for cDC1 and CD1c for cDC2, on human bone marrow cDCs (*n* = 3 donors). Data are gated on lineage$^-$ CD45$^+$ CD14$^-$ CD13$^+$ CD33$^+$ CD11c$^+$ HLA-DR$^+$ DCs. (**H**) Bone marrow DCs were sorted from *Cx3cr1*$^{gfp/+}$ mice as Gr-1$^-$ B220$^-$ MHC-II^{hi} CD11c^{hi} CX3CR1-GFP^{hi} cells. Heatmap comparing the expression of all chemokines and their receptors expressed in murine BM DCs and spleen (Sp) cDC2s (Gene Expression Omnibus database, accession no. GSE110789) (49). Data are mean ± SEM.

population of dendritic cells that have evolved to regulate hematopoiesis. We show that bone marrow DCs regulate endothelial cell function, in part, through CXCR2 signaling, resulting in HSPC mobilization and a loss of bone marrow macrophages. These findings establish bone marrow DCs as a new cellular component of the perivascular stem cell niche in both mice and humans.

Results

Bone marrow DCs are enriched in the perivascular region in mice and have a distinct phenotype. To better characterize bone marrow DCs, we developed a multicolor flow cytometry to analyze myeloid cell populations in *Cx3cr1*[gfp/+] mice, which express high levels of green fluorescent protein (GFP) in monocytes and bone marrow DCs, but not in bone marrow macrophages (9, 15, 16). Monocytes were identified as CX3CR1-GFP^{hi} MHC-II^{lo} Gr-1^{lo} B220^{−}/CD19^{−} cells (Figure 1A), and, consistent with a prior study, expressed F4/80 (17) but were mostly negative for CD11c and CD169 (Figure 1B). Bone marrow macrophages were identified as CX3CR1-GFP^{lo} MHC-II^{+} Gr-1^{lo} B220^{−}/CD19^{−} cells and expressed CD169 and F4/80, but little CD11c (Figure 1, A and B). Finally, bone marrow DCs were identified as CX3CR1-GFP^{hi} and MHC-II^{hi} Gr-1^{lo} B220^{−}/CD19^{−} cells. As expected, bone marrow DCs expressed a high level of CD11c and F4/80 (13), but a low level of CD169 (Figure 1, A and B). DCs represent 0.048% ± 0.017% of nucleated cells in mouse bone marrow compared with 0.096% ± 0.047% for macrophages (*n* = 11 mice). A prior study showed that bone marrow DCs are perivascular, although this study did not distinguish between venous sinusoids and arterioles (13). We show that CX3CR1-GFP[hi] and MHC-II[hi] DCs all have a stellate morphology (Figure 1C), enabling the identification of DCs as CX3CR1-GFP^{hi} stellate cells. We found that the great majority of these cells in the bone marrow are perivascular (Figure 1C), with approximately 90% of cells within 10 μm of a venous sinusoid or arteriole (Figure 1, D and E).

The high level of CD11c expression and stellate morphology of bone marrow DCs are consistent with cDCs (18, 19). To further characterize bone marrow DCs, we measured expression of XCR1 and CD11b, which are selectively expressed on cDC1s and cDC2s, respectively (20). For these experiments, cDCs were identified as Gr-1^{−} B220^{−} MHC-II^{hi} CD11c^{hi} cells. Nearly all of the DCs express CD11b but not XCR1, suggesting that the majority of murine bone marrow DCs are cDC2 cells (Figure 1F). Of note, consistent with a prior study (21), we observed that murine BM cDC2 cells express a higher level of CX3CR1-GFP than cDC1 cells (Supplemental Figure 1A; supplemental material available online with this article; https://doi.org/10.1172/JCI124829DS1). We next examined bone marrow from healthy donors to determine whether DCs also are present in human bone marrow. Human bone marrow DCs were identified as lineage^{−} CD45^{+} CD14^{−} CD13^{+} CD33^{+} CD11c^{+} HLA-DR^{+} cells (Supplemental Figure 1B). Indeed, the percentage of DCs in human bone marrow (0.082% ± 0.025%, *n* = 3 donors) is similar to that seen in murine bone marrow. Moreover, the majority of DCs in human bone marrow express CD1c but not CD141, and do not express CD45RA, consistent with a mature cDC2 phenotype (Figure 1G, and Supplemental Figure 1B) (20, 22). RNA expression profiling was performed on sorted murine bone marrow DCs and compared with prior data generated using splenic cDC2s. Surprisingly, the patterns of gene expression for chemokines, chemokine receptors, and certain DC marker genes were strikingly different, suggesting that bone marrow DCs may represent a unique dendritic cell population with distinct functional properties (Figure 1H and Supplemental Table 1).

Ablation of bone marrow DCs induces a loss of macrophages and HSPC mobilization. To assess their functional importance, bone marrow DCs were ablated using *Zbtb46*[dtr] mice. Recent studies have identified ZBTB46 as a transcription factor that is expressed in cDCs but not in plasmacytoid DCs (pDCs), macrophages, or other myeloid or lymphoid cells (23, 24). To confirm the specificity of *Zbtb46* expression in bone marrow DCs, we analyzed *Zbtb46*[gfp] mice, in which GFP is knocked into the *Zbtb46* locus (24). As expected, ZBTB46-GFP was expressed at high levels in bone marrow DCs, but not in bone marrow macrophages or monocytes (Figure 2A). Since endothelial cells also express *Zbtb46* (24), we transplanted *Zbtb46*[dtr] bone marrow into irradiated WT recipients to restrict *Zbtb46*[dtr] to the hematopoietic lineage. Diphtheria toxin (DT) treatment of *Zbtb46*[dtr] bone marrow chimeras resulted in a marked loss of bone marrow DCs (Figure 2B and Supplemental Figure 2A). Surprisingly, we also observed a loss of bone marrow macrophages (Figure 2B). However, the macrophage loss was delayed compared with cDC loss, raising the possibility that the decrease in macrophages is non–cell autonomous and secondary to cDC ablation. To test this possibility, we generated mixed bone marrow chimeras containing both WT and *Zbtb46*[dtr] hematopoietic cells. As expected, DT treatment resulted in the loss of *Zbtb46*[dtr]-derived but not WT-derived bone marrow cDCs (Figure 2C). In contrast, DT treatment resulted in decreases of both WT- and *Zbtb46*[dtr]-derived bone marrow macrophages (Figure 2D). Of note, DT treatment of WT mice did not result in a decrease in cDCs or macrophages in the bone marrow, nor did it induce HSPC mobilization (Supplemental Figure 2, B–E). Collectively, these data strongly suggest that cDC ablation results in a secondary, non–cell autonomous, loss of bone marrow macrophages.

We next assessed the impact of cDC ablation on HSPC trafficking. Ablation of bone marrow macrophages has been reported to alter the bone marrow niche and induce HSPC mobilization (9, 10). Thus, to determine whether bone marrow DCs have a macrophage-independent role in the regulation of HSPC trafficking, we compared HSPC mobilization after DT treatment in *Zbtb46*[dtr], *Cd169*[dtr], or *Zbtb46*[dtr] × *Cd169*[dtr] bone marrow chimeras. A prior study showed that *Cd169*[dtr] efficiently ablates bone marrow macrophages and results in modest HSPC mobilization (9). Treatment of *Zbtb46*[dtr] bone marrow chimeras with DT resulted in modest mobilization of CFU-C, c-kit^{+} Sca1^{+} lineage^{−} (KSL), and CD150^{+} CD48^{−} KSL (KSL-SLAM) cells (Figure 2, E–H), but did not affect HSPCs in the bone marrow (Supplemental Figure 3, A–C). Of note, DT treatment of *Zbtb46*[dtr] bone marrow chimeras did not result in an acute increase in blood or bone marrow neutrophils, or changes in bone marrow or spleen cellularity, suggesting that cDC ablation is not inducing systemic inflammation (Supplemental Figure 3, D–G). Importantly, the magnitude of HSPC mobilization in *Zbtb46*[dtr] bone marrow chimeras was significantly greater than that observed in *Cd169*[dtr] bone marrow chimeras but similar to that seen in the *Zbtb46*[dtr] × *Cd169*[dtr] bone marrow chimeras (Figure 2, E–H), suggesting that cDC ablation induces HSPC mobilization, at least in part, in a macrophage-independent fashion.
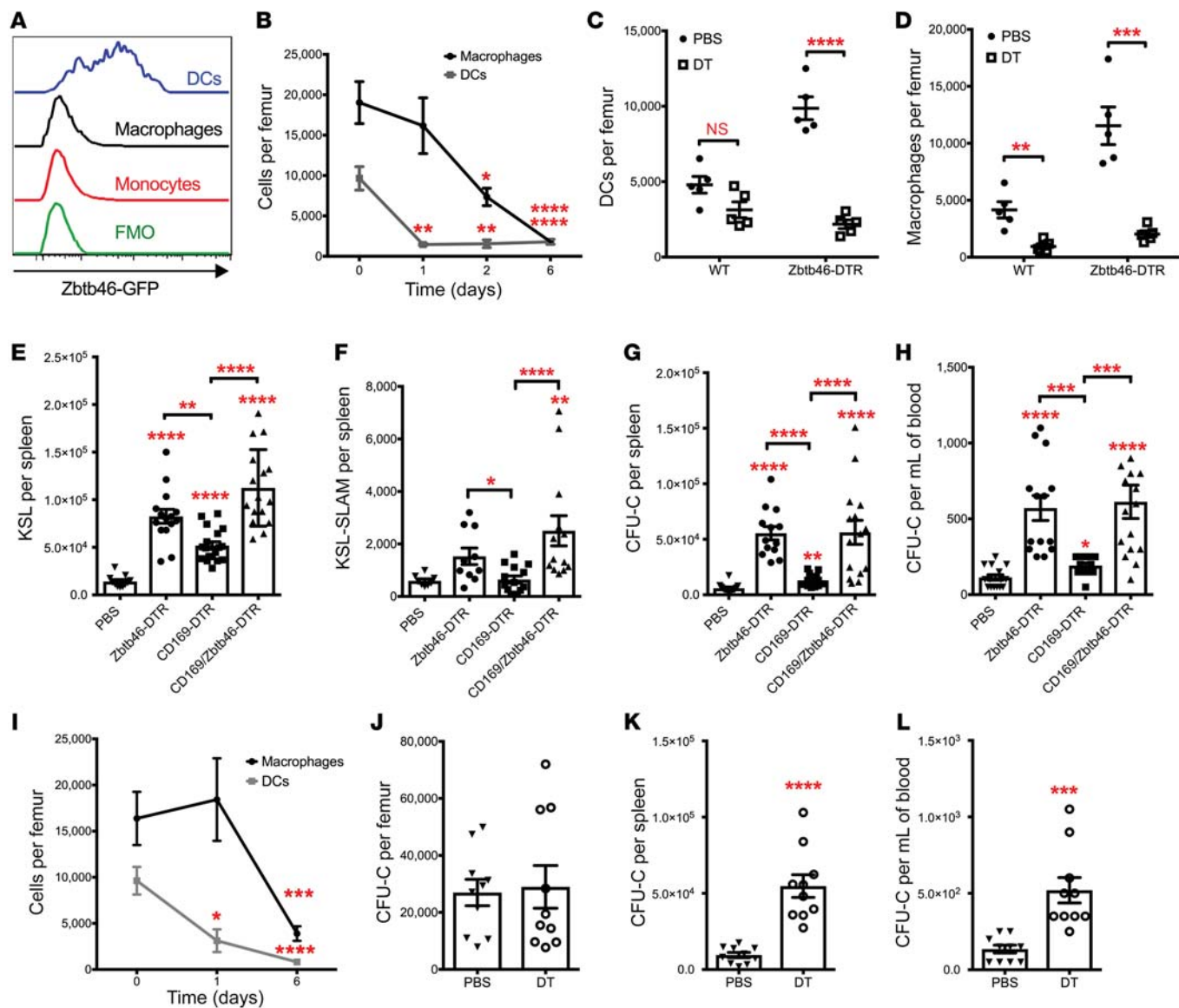
Figure 2. Bone marrow DC ablation induces a loss of macrophages and HSPC mobilization. (**A**) Expression of GFP in bone marrow monocytes (Gr-1^{lo} B220^{-} CD115^{+} cells), macrophages (Gr-1^{lo} B220^{-} MHC-II^{+} F4/80^{+} cells), and DCs (Gr-1^{lo} B220^{-} MHC-II^{hi} CD11c^{hi} cells) from *Zbtb46*[gfp] mice is shown. FMO, fluorescence minus one control. (**B**) *Zbtb46*[dtr] bone marrow chimeras were treated with DT for 1 day (*n* = 5 mice), 2 days (*n* = 5 mice), 6 days (*n* = 12 mice), or with PBS (day 0) (*n* = 11 mice), and BM DCs and macrophages were quantified. (**C**, **D**) Mixed bone marrow chimeras containing WT and *Zbtb46*[dtr] cells were treated with PBS or DT for 6 days, and the number of DCs (**C**) and macrophages (**D**) in the bone marrow that were derived from WT or *Zbtb46*[dtr] (Zbtb46-DTR) cells were quantified (*n* = 5 mice per cohort). (**E**–**H**) *Zbtb46*[dtr], *CD169*[dtr] (CD169-DTR), and *CD169*[dtr] × *Zbtb46*[dtr] (CD169/Zbtb46-DTR) chimeras were treated with PBS or DT for 6 days, and the number of lineage- sca1^{+} c-kit^{+} (KSL) cells (**E**) (*n* = 11, 15, 18, 16 mice) or CD150^{+} CD48^{-} KSL (KSL-SLAM) cells in the spleen (**F**) (*n* = 8, 10, 14, 13 mice) and the number of colony-forming cells (CFU-C) in spleen (**G**) (*n* = 14, 13, 12, 15 mice) or blood (**H**) (*n* = 15, 14, 12, 16 mice) were quantified. (**I**) *CD11c*[dtr] chimeras were treated with DT for 1 day (*n* = 3 mice), 6 days (*n* = 10 mice), or with PBS (*n* = 10 mice), and BM DCs and macrophages were quantified by flow cytometry. (**J**–**L**) *CD11c*[dtr] bone marrow chimeras were treated with saline or diphtheria toxin (DT) for 6 days, and the number of CFU-C in bone marrow (**J**), spleen (**K**), and blood (**L**) was quantified (*n* = 10 mice per cohort). Data are mean ± SEM. *$P < 0.05$; **$P < 0.01$; ***$P < 0.001$; ****$P < 0.0001$ compared with PBS-treated or day 0 mice. Significance was determined using an ANOVA with Tukey's Honest Significant Difference post hoc analysis for **C**, **E**–**H**, a 2-way ANOVA for **B**, **I**, or an unpaired Student's *t* test for **J**–**L**.

Zbtb46 is expressed in a subset of erythroid precursors (24). Indeed, DT treatment of *Zbtb46*[dtr] bone marrow chimeras resulted in a modest, but significant, decrease in basophilic erythroblasts, but not in later erythroid precursors (Supplemental Figure 3H) (25). Thus, we repeated the HSPC mobilization studies using *Cd11c*[dtr] mice, a mouse model of cDC ablation that does not target erythroid precursors (26). Similar to the *Zbtb46*[dtr] mice, DT treat-

ment of *Cd11c*[dtr] bone marrow chimeras resulted in the efficient ablation of DCs and a delayed loss of macrophages in the bone marrow (Figure 2I). Treatment of *Cd11c*[dtr] bone marrow chimeras with DT did not affect the number of HSPCs in the bone marrow (Figure 2J and Supplemental Figure 3I), but resulted in a modest mobilization of CFU-Cs and KSL cells (Figure 2, K and L, and Supplemental Figure 3J). The similar magnitude of bone marrow DC
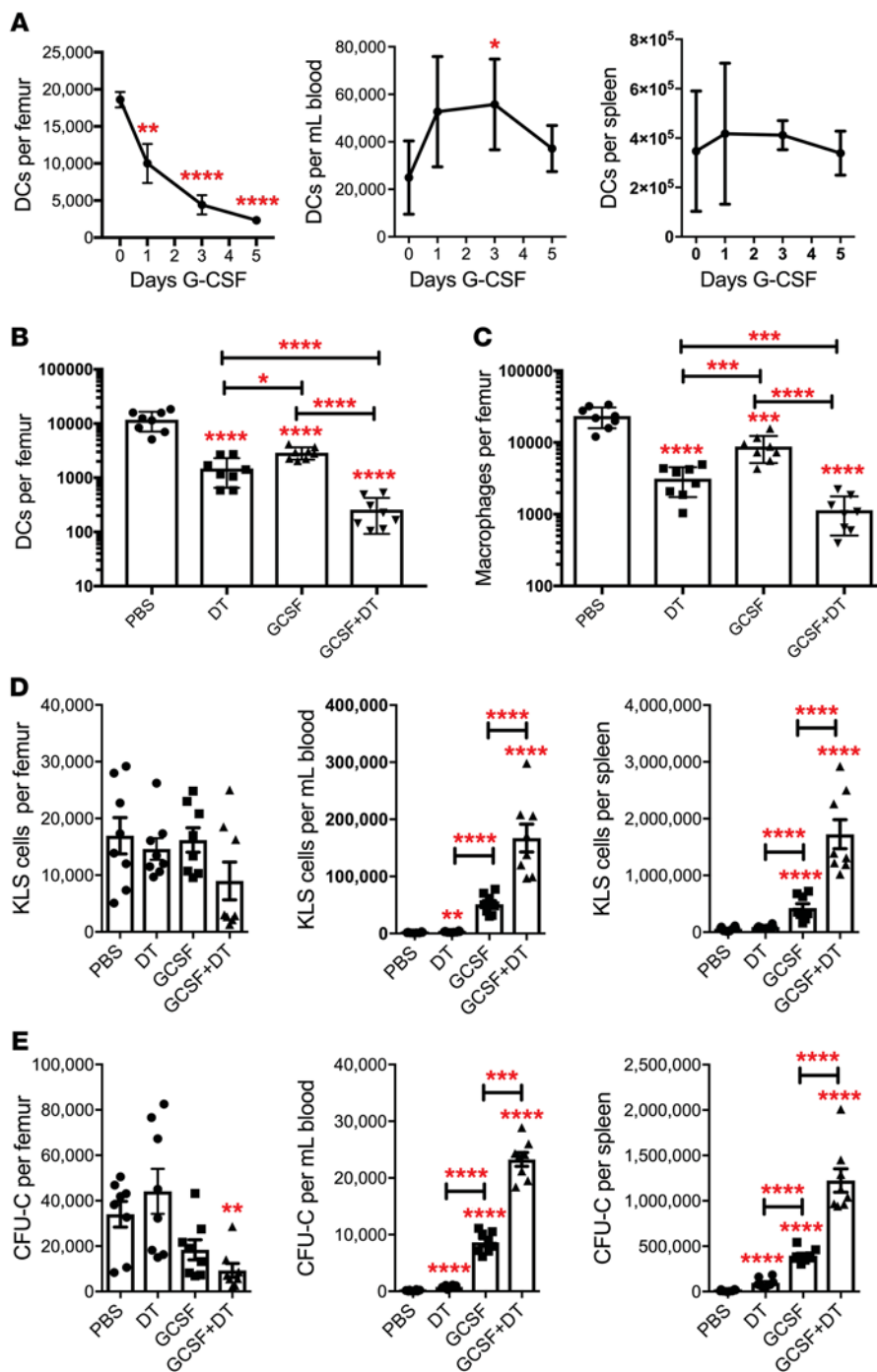
Figure 3. Bone marrow DC ablation synergizes with G-CSF to mobilize HSPCs. (**A**) Mice were treated with 250 μg/kg G-CSF daily for 5 days. Shown are the number of cDCs in the bone marrow, blood, and spleen (*n* = 5, 4, 4 and 6 mice per time point). (**B**–**E**) Mice were treated with saline alone (PBS), G-CSF for 5 days, or the combination of DT and G-CSF for 5 days (*n* = 8 mice per cohort). The number of cDCs (**B**) and macrophages (**C**) in the bone marrow is shown. The number of KSL (**D**) or CFU-C (**E**) in bone marrow, blood, and spleen are shown. Data are mean ± SEM. *$P < 0.05$; **$P < 0.0$; ***$P < 0.001$; ****$P < 0.0001$ compared with saline-treated mice. Significance was determined using a 2-way ANOVA for A or an ANOVA with Tukey's Honest Significant Difference post hoc analysis for **B**–**E**.

imaging of bone sections of *Cx3cr1*$^{gfp/+}$ mice (Supplemental Figure 4). Modest cDC mobilization also was observed after treatment with AMD3100, a CXCR4 antagonist (Supplemental Figure 5). Compared with splenic cDC2s, bone marrow cDCs express a higher level of *Csf3r*, which encodes for the G-CSF receptor (Supplemental Table 1). To assess the contribution of G-CSF signaling in cDCs to HSPC mobilization, we characterized G-CSF–induced HSPC mobilization in *Zbtb46*^{dtr} bone marrow chimeras after cDC ablation. As expected, both G-CSF and cDC ablation resulted in a significant decrease in bone marrow cDCs and macrophages, with the lowest levels of these cells observed after combined G-CSF and cDC ablation (Figure 3, B and C). Ablation of cDCs alone induced modest HSPC mobilization compared with G-CSF (Figure 3, D and E). However, the combination of cDC ablation and G-CSF treatment resulted in synergistic HSPC mobilization that was approximately 3-fold greater than that observed with G-CSF alone.

Ablation of bone marrow DCs induces endothelial cell expansion and increased vascular permeability in the bone marrow. The close physical association of bone marrow

ablation and HSPC mobilization in the *Zbtb46*^{dtr} and *Cd11c*^{dtr} chimeras strongly suggests that it is the loss of DCs that is responsible for HSPC mobilization in these mice.

Ablation of bone marrow DCs synergizes with G-CSF to mobilize HSPCs. We previously showed that G-CSF treatment is associated with a marked decline of monocytes in the bone marrow (8). Using our multicolor flow assay, we quantified cDCs in the bone marrow, peripheral blood, and spleen at baseline and following G-CSF treatment (Figure 3A). G-CSF treatment is associated with a 6.8-fold decrease in cDCs in the bone marrow, while they are modestly increased in the blood, suggesting that cDCs are mobilized by G-CSF. The decrease in bone marrow cDCs was confirmed by

DCs with sinusoidal endothelium, the site where most HSPC transmigration is thought to occur, prompted us to examine endothelial cell function following cDC ablation. We first assessed bone marrow vascular permeability, since it has been reported to positively affect HSPC mobilization in the bone marrow (27–29). Fluorescein-conjugated bovine serum albumin (FITC-BSA) was injected intravenously into *Zbtb46*^{dtr} bone marrow chimeras following DT treatment. Mice were harvested after 15 minutes and immunostaining of femur sections was performed to quantify extravascular and intravascular FITC-BSA, as previously described (Figure 4A) (30). A modest but significant increase in vascular permeability was observed after 6 days of DT treatment (Figure 4C). We also
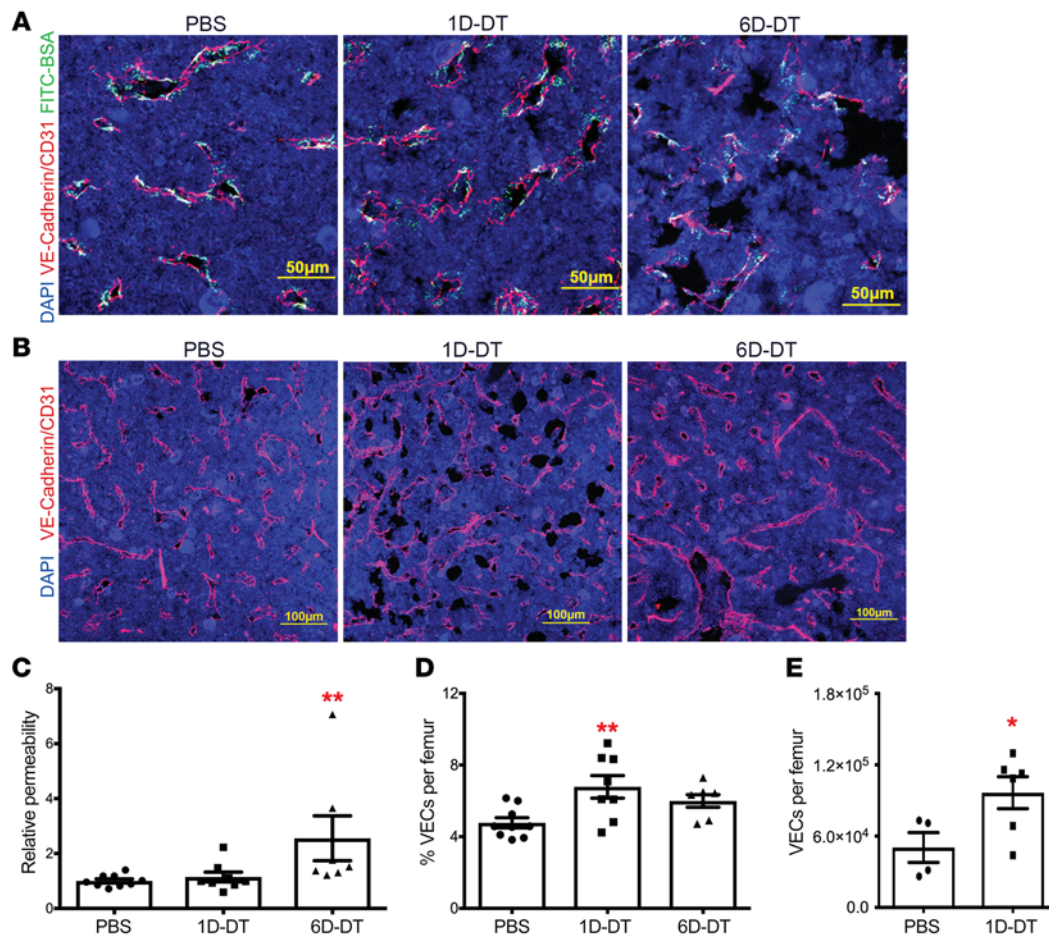
Figure 4. Bone marrow DC ablation induces vascular endothelium permeability and expansion in the bone marrow. (**A**, **B**) Representative photomicrographs of femur sections from *Zbtb46*^{dtr} bone marrow chimeras treated with PBS (left), 1 day of DT (1D-DT, middle) or 6 days of DT (6D-DT, right). (**A**) FITC-conjugated bovine serum albumin (BSA) was injected intravenously into mice 15 minutes before sacrifice. Sections were imaged for FITC-BSA (green) and VE-cadherin$^+$/CD31$^+$ endothelial cells (red). (**B**) Sections were imaged for VE-cadherin$^+$/CD31$^+$ endothelial cells (red) and counterstained with DAPI to highlight nuclei (blue). Original magnification, ×200. (**C**) The ratio of extravascular FITC-BSA to intravascular FITC-BSA was quantified and normalized to the PBS-treated cohort (n = 9, 8, 7 mice). (**D**, **E**) Histomorphometry (**D**) (n = 9, 8, 7 mice) or flow cytometry (**E**) (n = 4 or 6 mice) was used to quantify endothelium or endothelial cells in the bone marrow; endothelial cells were identified by flow cytometry as lineage$^-$ (CD45, Ter119, Gr-1) CD31$^+$ cells. Data are mean ± SEM. *P < 0.05; **P < 0.01 compared with PBS-treated mice. Significance was determined using an ANOVA with Tukey's Honest Significant Difference post hoc analysis for **C** and **D**, or an unpaired Student's t test for **E**.

observed a significant expansion of vascular endothelial cells by immunostaining (Figure 4, B and D) and flow cytometry (Figure 4E) after cDC ablation. To further characterize alterations in the bone marrow vasculature, sinusoidal (lineage$^-$ CD31$^+$ Sca1$^-$) and arteriolar (lineage$^-$ CD31$^+$ Sca1$^+$) endothelial cells were flow sorted from *Zbtb46*^{dtr} bone marrow chimeras 1 day after DT treatment, a time when bone marrow DCs, but not macrophages, are decreased in the bone marrow (Supplemental Figure 6A). RNA expression profiling was performed on the sorted populations. Principal component analysis (PCA) showed that sinusoidal but not arteriolar endothelial cells clustered based on cDC ablation (Supplemental Figure 6, B and C). To better characterize transcriptional changes associated with cDC ablation, we performed RNA sequencing on sorted bone marrow sinusoidal endothelial cells. The data were analyzed using t-distributed stochastic neighbor embedding (t-SNE) and, again, showed that cells clustered based on cDC ablation (Figure 5A). A total of 635 differentially expressed genes (> 5-fold difference and FDR < 0.02) were identi-

fied (Supplemental Table 2). Gene set enrichment analysis (GSEA) was performed and the top hit was related to chemokine/cytokine activation (Figure 5B). GSEA also suggested increased angiogenesis (Figure 5C), which is consistent with the modest expansion of vascular endothelial cells seen after cDC ablation. Collectively, these data show that cDC ablation results in vascular remodeling in the bone marrow, including modest angiogenesis and increased vascular permeability.

Ablation of bone marrow DCs may regulate HSPC trafficking partially through activation of sinusoidal CXCR2 signaling. Among the most highly induced genes in sinusoidal endothelial cells following cDC ablation are certain chemokine receptors, including CCR1, CCR2, and CXCR2 (Figure 5D). CXCR2 is of particular interest, since prior studies have suggested that CXCR2 activation induces vascular permeability and HSPC mobilization (29, 31–33). We performed real-time quantitative PCR on whole bone marrow RNA from *Zbtb46*^{dtr} bone marrow chimeras following DT treatment to measure the expression of CXCL1 (KC) and CXCL2 (Gro-β), the
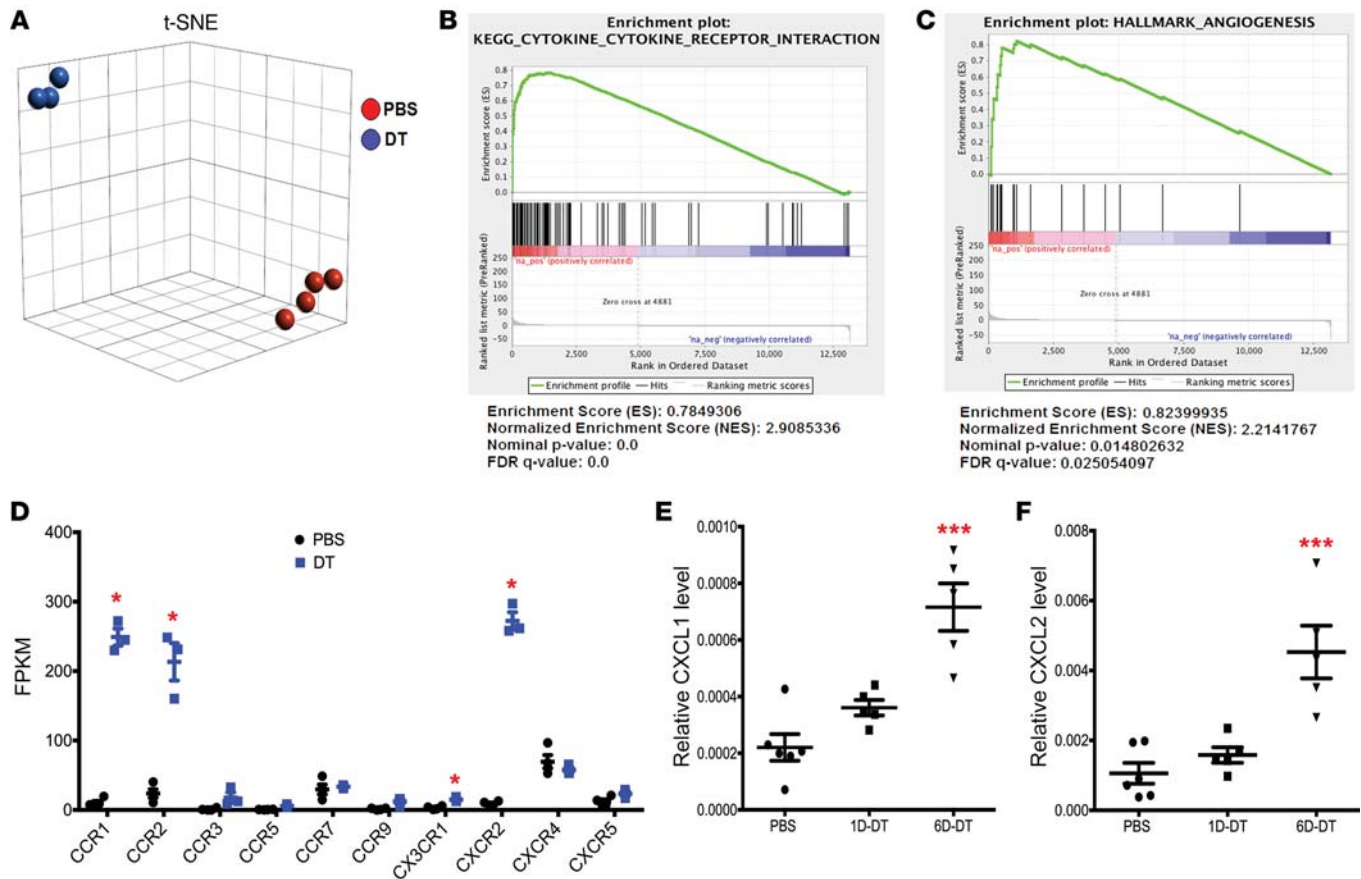
Figure 5. Ablation of bone marrow DCs activates sinusoidal endothelial cells. (**A**) Sinusoidal endothelial cells were sorted from *Zbtb46^dtr* bone marrow chimeras treated with PBS or DT (1 day) and RNA-sequencing was performed. t-SNE analysis of PBS- (*n* = 4 mice) and DT-treated mice (*n* = 3 mice). (**B**, **C**) Gene set enrichment analysis (GSEA). (**D**) Fragments per kilobase (FPKM) values for all expressed chemokine receptors in sinusoidal endothelial cells. *False discovery rate < 0.05. Significance was determined using the Partek gene-specific analysis (GSA) algorithm. (**E**, **F**) Expression of CXCL1 (**E**) and CXCL2 (**F**) mRNA relative to β-actin mRNA in the bone marrow of *Zbtb46^dtr* chimeras following treatment with PBS (*n* = 6 mice) or DT for 1 day (1D-DT, *n* = 5 mice) or 6 days (6D-DT, *n* = 5 mice). Data are mean ± SEM. ***$P < 0.001$ compared with PBS-treated mice. Significance was determined using ANOVA with Tukey's Honest Significant Difference post hoc analysis for **E** and **F**.

principal ligands for CXCR2. RNA expression of both ligands was induced 3- to 4-fold in the bone marrow following cDC ablation (Figure 5, E and F). To directly test the effect of CXCR2 activation on endothelial cells, we performed transwell experiments using a human umbilical vein endothelial cell (HUVEC) monolayer (Figure 6A). Vascular permeability, as measured by Evans blue passage into the bottom chamber was modestly, but significantly, increased by treatment with recombinant CXCL1 (Figure 6B). Likewise, CXCL1 treatment increased the migration of human CD34+ cells through a HUVEC monolayer (Figure 6C). To assess the impact of endothelial CXCR2 signaling in vivo, we transplanted *Zbtb46^dtr* bone marrow into irradiated *Cxcr2^-/-* recipients, thereby restricting the loss of CXCR2 signaling to endothelial cells and other stromal cells. Compared with WT recipients, mobilization of KSL cells, KSL-SLAM cells, and CFU-Cs was significantly reduced in *Cxcr2^-/-* recipients following cDC ablation (Figure 6, G, I, K, L and Supplemental Figure 7). Of note, cDC ablation in *Cxcr2^-/-* recipients did not alter bone marrow or spleen cellularity, or HSPC numbers in the bone marrow (Figure 6, D–F, H, and J). Collectively, these data suggest that cDC ablation induces HSPC mobilization, in part, through CXCR2 activation in bone marrow sinusoidal endothelial cells.

Discussion

Consistent with a prior study by Sapoznikov and colleagues, we identified a resident population of DCs that localize to both venous sinusoids and arterioles in the bone marrow (13). The majority of bone marrow DCs are CD11b+ and XCR1–, classifying them as cDC2-like cells. We identified a similar population of cDC2-like cells in human bone marrow. Several recent studies using single-cell analysis platforms show that there is considerable heterogeneity within the DC population, suggesting that current classification schemes may need to be expanded (22, 34–36). Our RNA expression profiling data suggest that bone marrow cDCs have a distinct pattern of gene expression. For instance, while certain cDC2 genes are highly expressed in bone marrow cDC2 cells, such as *Cx3cr1* and *Fcgr1*, certain cDC1 genes are also highly expressed, such as *Irf8* and *Clec9a* (Supplemental Table 1). There also is considerable heterogeneity in the expression of chemokine, cytokine, and pattern recognition receptors in cDC2 cells from different tissues, which contributes to their functional diversity (11). Indeed, striking differences in chemokine receptor and toll-like receptor expression were observed between splenic cDC2s to bone marrow cDC2s, with bone marrow cDC2s typically showing
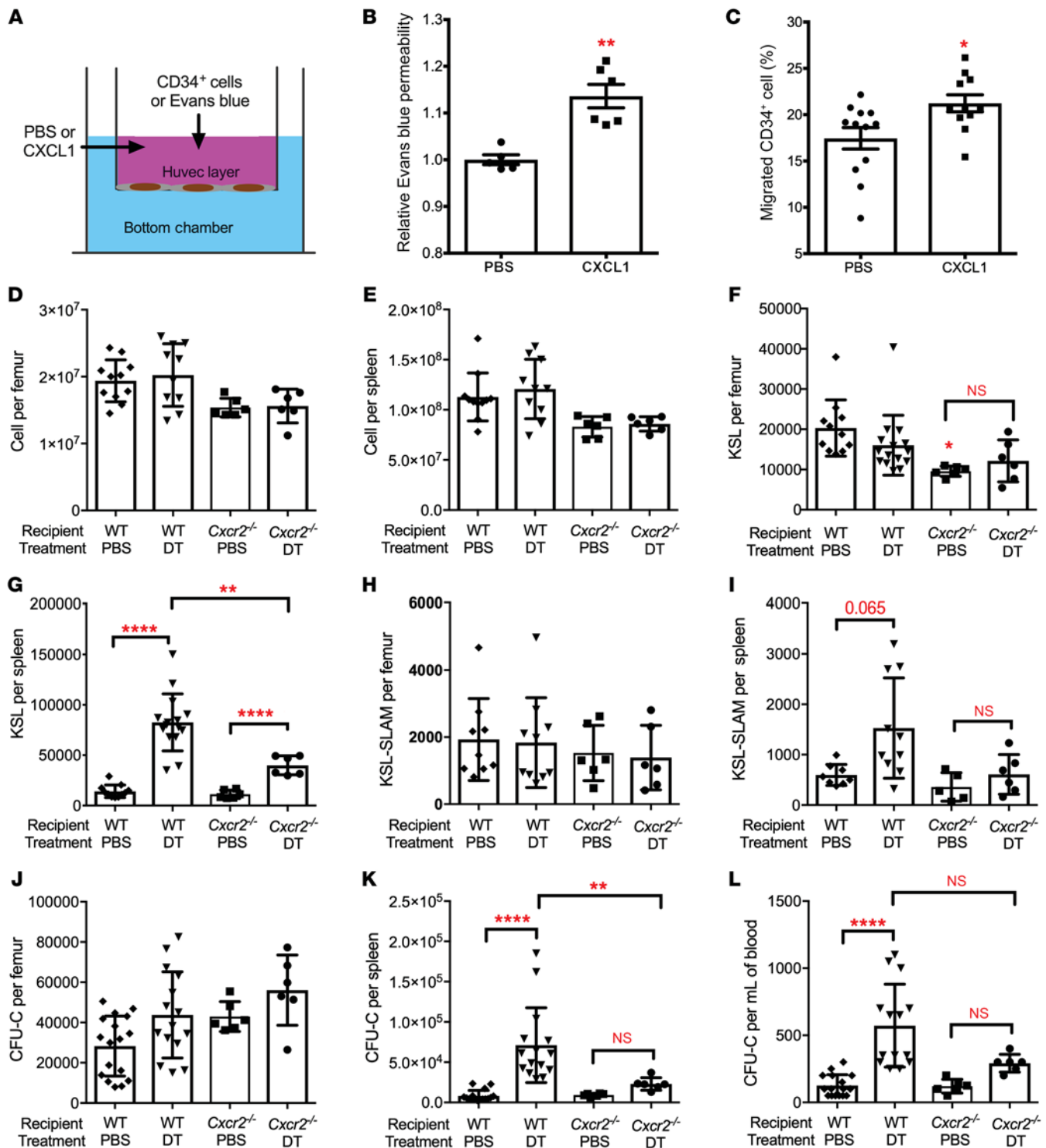
Figure 6. CXCR2 signaling contributes to HSPC mobilization following bone marrow DC ablation. (A–C) Human umbilical vein endothelial cells (HUVECs) cultured in a transwell to establish a monolayer were treated with PBS or CXCL1. **(B)** Relative amount of Evans blue dye in the lower chamber after 1 hour of CXCL1; data are normalized to PBS-treated samples (*n* = 5 or 6 mice). **(C)** Human bone marrow CD34+ cells were seeded on the HUVEC monolayer and treated with CXCL1 for 24 hours; the lower chamber contained 100 ng/ml CXCL12. Shown is the percentage of CD34+ cells that migrated to the lower chamber (*n* = 11–12 replicates). **(D–L)** Bone marrow cells from *Zbtb46*[dtr] mice were transplanted into irradiated WT or *Cxcr2*^{−/−} recipients. Eight weeks after transplantation, mice were treated with PBS or DT for 6 days. Total cellularity of bone marrow **(D)** and spleen **(E)**, the number of KSL cells in bone marrow **(F)** and spleen **(G)**, the number of KSL-SLAM cells in bone marrow **(H)** and spleen **(I)**, and the number of CFU-Cs in bone marrow **(J)**, spleen **(K)**, and blood **(L)** is shown (*n* = 6 per cohort). The WT recipient data are the same as shown in Figure 2. Data are mean ± SEM. *$P < 0.05$; **$P < 0.01$; ****$P < 0.0001$ compared with the PBS-treated group, unless otherwise specified. Significance was determined using an unpaired Student's *t* test for **B** and **C**, or ANOVA with Tukey's Honest Significant Difference post hoc analysis for **D–L**.

higher expression. Collectively, these data suggest that bone marrow cDC2s may represent a unique dendritic cell population that has evolved to perform specialized functions.

We show that cDC ablation using either *Zbtb46^dtr* or *Cd11c^dtr* transgenic mice results in a loss of bone marrow macrophages and mobilization of HSPCs. Analysis of *Zbtb46^dtr* bone marrow chimeras establishes that the macrophage loss is non–cell autonomous. The mechanism(s) by which cDCs regulate bone marrow macrophages is uncertain and will require further study. However, it is noteworthy that bone marrow DCs express high levels of CCL6 (Figure 1H), which is known to regulate the migration and activation of macrophages (16). A prior study showed that ablation of CD169+ macrophages induces modest HSPC mobilization (9). Indeed, we observed weak HSPC mobilization in our *Cd169^dtr* bone marrow chimeras following macrophage ablation. However, HSPC mobilization was significantly greater after cDC ablation, and no significant increase in HSPC mobilization was observed with combined macrophage and cDC ablation compared with cDC ablation alone. These data suggest that bone marrow DCs regulate HSPC trafficking in a macrophage-independent fashion.

We previously reported that G-CSF signaling in monocytic-lineage cells is sufficient to mediate G-CSF–induced HSPC mobilization (8). Within the monocytic-lineage cell population, the G-CSF receptor is expressed on monocytes, macrophages, and, based on our RNA expression data, bone marrow cDCs. Here, we show that cDC ablation synergizes with G-CSF to mobilize HSPCs, demonstrating that G-CSF signaling in cDCs is not required for HSPC mobilization. A prior study showed that Gro-β, a CXCR2 ligand, synergizes with G-CSF to induce HSPC mobilization (37). We show that cDC ablation induces expression of the CXCR2 ligands CXCL1 and CXCL2 in the bone marrow. Thus, one potential mechanism for the synergistic mobilization with G-CSF is the stimulation of CXCR2 signaling in the bone marrow following cDC ablation.

Our data suggest that DCs regulate endothelial cell function in the bone marrow. The great majority of bone marrow DCs are in direct contact with bone marrow endothelial cells. Ablation of cDCs results in endothelial cell expansion and increased vascular permeability. Finally, cDC ablation is associated with rapid (within 24 hours) changes in sinusoidal endothelium gene expression, suggesting chemokine/cytokine activation and angiogenesis. These observations are consistent with prior studies showing that cDCs play an important role in inflammatory angiogenesis and lymphangiogenesis, possibly through vascular endothelial growth factor A (VEGFA) production (38, 39). On the other hand, perivascular macrophages have been implicated in the regulation of vascular permeability (40). Interestingly, the increase in vascular permeability following cDC ablation was delayed, similar to that observed for the loss of bone marrow macrophages. Whether it is the loss of macrophages that mediates the increase in vascular permeability following cDC ablation will require further study.

We provide evidence that cDC ablation induces HSPC mobilization, in part, by inducing CXCR2 signaling in endothelial cells. Following cDC ablation, CXCR2 expression in sinusoidal endothelial cells increases, as does bone marrow expression of the CXCR2 ligands CXCL1 and CXCL2. The cellular source of the increased CXCL1 and CXCL2 expression and the mechanisms for the increased endothelial CXCR2 expression are unclear and

will require further study. Treatment with CXCL1 induces vascular permeability and transendothelial migration of HSPCs in vitro. Moreover, HSPC mobilization following cDC ablation is attenuated in mice lacking endothelial CXCR2 expression. These observations are consistent with a report by Hoggatt and colleagues showing that treatment with a CXCR2 agonist induces bone marrow vascular permeability and HSPC mobilization (29). It is also consistent with a companion paper by Karpova and colleagues showing that CXCR2 agonist–induced HSPC mobilization is dependent, in part, on CXCR2 signaling in endothelial cells (41). However, in the *Zbtb46^dtr Cxcr2^-/-* chimeras, CXCR2 expression is abrogated in all bone marrow stromal cells, raising the possibility that CXCR2 signaling in nonendothelial stromal cells contributes to HSPC mobilization. The residual HSPC mobilization in *Cxcr2^-/-* recipients also suggests that there are non–CXCR2-dependent mechanisms that contribute to HSPC mobilization following cDC ablation. These mechanisms will require further investigation, but it is noteworthy that CCR1 and CCR2 are highly induced on sinusoidal endothelial cells following cDC ablation, and signaling from both of these receptors has been implicated in the regulation of endothelial cell function (42–44).

In summary, these data show that bone marrow DCs are an important cellular component of the perivascular hematopoietic niche. Their perivascular location and high expression of certain chemokine and pattern recognition receptors suggest that bone marrow DCs may play an important role in sensing and regulating the hematopoietic response to microbes and inflammatory signals.

Methods

Mice. The *Cxcr1^gfp/+* mice were a gift from David Littmann (New York University School of Medicine) (15). *Zbtb46^dtr* (*B6(Cg)-Zbtb46^tm1(HBEGF)Mnz/J*), *Zbtb46^gfp* (129S-Zbtb46^tm1Kmm/J), and *Cxcr2^-/-* (*C.129S2(B6)-Cxcr2^tm1Mwm/J*) mice were obtained from The Jackson Laboratory. *Cd169^dtr* mice were a gift from Y. Obata (Riken BioResource Center, Ibaraki, Japan) (45, 46). *Cd169^dtr* mice were bred with *Zbtb46^dtr* mice to generate *Cd169^dtr* × *Zbtb46^dtr* mice. Sex- and age-matched mice were used in all experiments. All mice were inbred on a C57BL/6 background except *Zbtb46^gfp* mice, which were on a mixed C57BL/6 and 129 SvEv background. The number of animals used per experiment is stated in the figure legends. Mice were maintained under SPF conditions, and all experimental procedures were performed according to methods approved by the Animal Studies Committee at Washington University.

Generation of bone marrow chimeras. Six- to eight-week-old WT *Ly5.1/Ly5.2* recipient mice were irradiated with two 600 cGy doses, 6 hours apart. Two million donor bone marrow cells were then retro-orbitally injected. Mice were placed on prophylactic antibiotics (trimethoprim-sulfamethoxazole) for 2 weeks following the first dose of irradiation. Mice were analyzed 8 weeks after transplantation.

Diphtheria toxin, G-CSF, and AMD3100 administration. Diphtheria toxin (D0564, MilliporeSigma) was diluted in PBS containing 0.1% low-endotoxin BSA and administered intraperitoneally at a dose of 200 ng/mouse/day for up to 6 days. G-CSF (neupogen, Amgen) was diluted in sterile PBC containing 0.1% low-endotoxin BSA and administered subcutaneously at a dose of 250 μg/kg/day for 5 days. AMD3100 (MilliporeSigma) was diluted in sterile PBS containing 0.1% low-endotoxin BSA and administered subcutaneously at a dose of 5 mg/kg.

CFU-C assays. Cells obtained from the bone marrow, peripheral blood, and spleen were analyzed using a Hemavet automated cell counter (Drew Scientific). Peripheral blood (40 μl), bone marrow cells (2.5×10^4), or splenic cells (1.0×10^5) were suspended in 3 ml Mouse Methylcellulose Complete Media (HSC007, R&D Systems). Cell suspensions were plated in duplicate in 60-mm petri dishes and incubated in a humidified chamber with 5% CO_2 at 37°C. The number of colonies per dish was counted on day 7.

Flow cytometry. Bone marrow, spleen, and peripheral blood were processed for flow cytometry as previously described (47). Cells were analyzed on a Gallios flow cytometer (Beckman Coulter) or sorted using a Sony SY3200 Synergy high-speed cell sorter (Sony). Data analysis was done using FlowJo version 10.0.7 software (TreeStar). The following antibodies were used for staining murine cells: Gr-1 (clone RB6-8C5), CD19 (clone 1D3), CD48 (clone BCM1), B220 (clone RA3-6B2), CD3e (clone 17A2), Ter119 (clone TER-119), Sca-1 (clone D7), CD117 (clone 2B8), CD115 (clone AFS98), CD45 (clone 30-F11), CD45.1 (clone A20) and CD45.2 (clone 104), all from eBiosciences; CD31 (clone 390), F4/80 (clone BM8), I-A/I-E (clone M5/114.15.2), CD11c (clone N418), CD150 (clone TC15-12F12.2), CD169 (clone 3D6.112), CD11b (clone M1/70), and XCR1 (clone ZET) from BioLegend; and CD71 (clone C2) from BD Biosciences.

For cell sorting, dendritic cells from bone marrow and spleen were identified as CX3CR1-GFP^{hi} B220$^-$ Gr-1$^-$ MHC-II^{hi} CD11c^{hi} cells. Sinusoidal endothelial cells were identified as lineage$^-$ (CD45$^-$ Ter119$^-$ Gr-1$^-$) CD31$^+$ Sca1$^-$ cells, and arteriolar endothelial cells were identified as lineage$^-$ CD31$^+$ Sca1$^+$ cells.

For human bone marrow cells, dendritic cells were identified as lineage$^-$ (CD3, CD15, CD19, CD20, CD56) CD45$^+$ CD13$^+$ CD14$^-$ CD33$^+$ CD11c$^+$ HLA-DR$^+$ cells. The following antibodies were used: CD3 (clone 555332), CD15 (clone 555401), CD19 (clone 555412), CD11c (clone B-ly6), and CD45RA (clone L48) from BD Biosciences; CD13 (clone WM-15), CD20 (clone 2H7), and CD56 (clone MEM188) from eBiosciences; CD33 (clone P67.6), CD1c (clone L161), CD14 (clone M5E2), CD141 (clone M80), and HLA-DR (clone L243) from BioLegend.

Immunostaining of bone sections. Mouse hind limbs were processed for immunostaining as previously described (48). The following antibodies were used: chicken anti-GFP (ab13970, Abcam), rat anti–MHC-II (107601, BioLegend), rat anti-Sca1 (557403, BD Biosciences), goat anti–VE-cadherin (AF1002, R&D Systems), and anti-B220 (12-0452-83, eBioscience); Alexa Fluor 488 donkey anti-rat IgG (Invitrogen), Alexa Fluor 488 donkey anti-chicken IgG (Jackson Immunoresearch), and biotin-conjugated donkey anti-goat IgG (Jackson Immunoresearch). In some cases, slides were then incubated with streptavidin-DyLight 649 (Jackson Immunoresearch) for 30 minutes at room temperature. Finally, slides were mounted with Pro-Long Gold antifade reagent with DAPI (Life Technologies). Images were acquired with an LSM 700 microscope (Carl Zeiss), and images were processed using Volocity software (Perkin Elmer).

Histomorphometry was used to quantify the distance of bone marrow DCs to the vasculature using CX3CR1-GFP mice. The distance of GFP-bright reticular-shaped DCs to VE-cadherin$^+$ Sca1$^-$ sinusoidal endothelial cells or VE-cadherin$^+$ Sca1$^+$ arteriolar endothelial cells was quantified using Volocity software (Quorum Technologies). Specifically, the distance from the center of the DCs (identified manually) to the nearest border of the closest endothelial cell was measured.

In vivo FITC-BSA permeability assay. FITC-conjugated BSA (FITC-BSA), 0.5 mg in 50 μl PBS, was intravenously injected into *Zbtb46^{dtr}* bone marrow chimeras, and 15 minutes after injection their femurs were fixed and processed for immunostaining. Intravascular FITC-BSA was identified as an FITC signal that localized inside of VE-cadherin$^+$ blood vessels. Extravascular FITC-BSA was identified as an FITC signal outside bone marrow vasculature, but in the bone marrow. Both intravascular and extravascular FITC-BSA was quantified using Volocity software. Permeability was calculated as: permeability = (extravascular FITC-BSA – background) / (intravascular FITC-BSA – background).

Real-time quantitative RT-PCR. Mouse femurs were flushed with 1 ml TRIzol reagent (Invitrogen) and RNA was isolated according to the manufacturer's instructions. Reverse transcription was performed using the iScript cDNA Synthesis Kit (Bio-Rad) according to the manufacturer's instructions. Quantitative PCR was performed using the iTaq Universal Probes Supermix (Bio-Rad) on a StepOne Plus Real-Time PCR System (Applied Biosystems). RNA content was normalized to mouse β-actin. Primer and probes for mouse β-actin (Mm01324804_m1), CXCL1 (Mm04207460_m1), and CXCL2 (Mm00436450_m1) were ordered from Thermo Fisher Scientific.

RNA expression profiling. RNA was purified from sorted dendritic cells and endothelial cells using the Qiagen RNeasy Micro Kit (74004, Qiagen Technologies). For RNA microarray, libraries were generated using the NuGen Pico SL kit (NuGen Technologies) and then hybridized to Affymetrix Mouse Gene 1.0 ST arrays (Affymetrix). Biotinylated cDNA was prepared according to the Affymetrix WT Pico reagent kit from total RNA. Following fragmentation and labeling, cDNA was hybridized onto Affymetrix Clariom S arrays and placed in a GeneChip Hybridization Oven 640. GeneChips were then washed and stained in an Affymetrix Fluidics Station 450. GeneChips were scanned using the Affymetrix GeneChip 7G 3000 Scanner. Data were analyzed on an Affymetrix GeneChip Command Console. Microarray expression data were processed using the Command Console (Affymetrix) and the raw (.CEL) files generated were analyzed using Expression Console software with Affymetrix default RMA Gene Analysis settings. Probe summarization (Robust Multichip Analysis, RMA), quality control analysis, and probe annotation were performed according to the recommended guidelines (Expression Console software, Affymetrix). Gene set enrichment was performed using the GSEA software (Broad Institute). Heatmap was performed using R package (version 3.4.4).

For RNA sequencing, library preparation was performed with 1 ng of total RNA using the SMARTer Ultra Low RNA kit for Illumina Sequencing (Clontech) per the manufacturer's protocol. The resulting cDNA was fragmented to 150–550 bp using a Covaris E220 sonicator (Covaris), then ligated with Illumina sequencing adapters, and amplified to incorporate unique index tags. Fragments were sequenced on an Illumina HiSeq-3000 (Illumina) using single reads extending 50 bases. All data from RNA sequencing were analyzed using Partek Flow software, version 7.0 (Partek). Reads were aligned to the mm10 mouse reference genome by STAR (v. 2.5.3a) and normalized FPKM values were determined using Partek E/M (mm10 Ensembl Transcripts release 88). The Partek gene specific analysis (GSA) algorithm was utilized for differential expression analyses. t-SNE plots were performed using Partek.

In vitro permeability test and cell migration assay. HUVECs (S200-05N, MilliporeSigma) were cultured in Endothelial Cell Growth Medium (211-500, MilliporeSigma) at 37°C, 5% CO_2. HUVECs (2×10^5) were precultured in the upper chamber of the Boyden Chamber

system for 24 hours to form a HUVEC layer. During the same time, the HUVEC layer was pretreated with 40 ng/ml recombinant CXCL1 (453-KC-010/CF, Thermo Fisher Scientific) or PBS as a control.

To test permeability of the HUVEC layer, 400 μl Endothelial Cell Growth Medium containing 100 μg/ml Evans blue was added to the upper chamber of the cell insert with 0.4 μm pores in the membrane (141078, Thermo Fisher Scientific). Hank balanced salt solution (1 ml, H6648-500ML, MilliporeSigma) was added to the bottom chamber. After 1 hour incubation at 37°C, 5% CO_2, Evans blue in the bottom chamber was measured by light absorbance at 620 nm using an Epoch 2 microplate spectrophotometer (Biotek), and the amount of Evans blue was calculated using a standard curve. Amount of Evans blue in the CXCL1-treated samples was normalized to the amount in the PBS-treated control samples for comparison.

To test cell migration through the HUVEC layer, 400 μl medium containing approximately 5×10^4 human CD34+ cells was added to the upper chamber of the cell insert with 3 μm pores in the membrane (141080, Thermo Fisher Scientific); the bottom chamber contained 100 ng/ml recombinant CXCL12 (578702, BioLegend). Human CD34+ cells were enriched from primary human bone marrow donated by healthy donors using the CD34 MicroBead Kit (130-100-453, Miltenyi Biotec) and autoMACS Pro Separator (Miltenyi Biotec). In some cases, the HUVEC layer was treated for 24 hours with CXCL1 or PBS prior to the addition of CD34+ cells. The number of cells in the bottom chamber after a 24-hour incubation at 37°C was quantified using a Cellometer Auto T4 Bright Field Cell Counter (Nexcelom).

Statistics. Statistical significance was determined using Prism 6.0 software (GraphPad). Unpaired *t* test, 2-way ANOVA, or ANOVA with Tukey's Honest Significant Difference post hoc analysis was used to evaluate the significance of differences between 2 or multiple groups. All data are mean ± SEM.

Study approval. All animal studies were approved by the Institutional Animal Care and Use Committee at Washington University, St. Louis, Missouri, USA.

Data availability. RNA expression data for bone marrow DCs and the RNA-seq data for sinusoidal endothelial cells have been submitted to the Gene Expression Omnibus database (GSE112082, GSE118017, respectively).

Author contributions

JZ, MR, and DCL conceived of this study. JZ and TS performed the majority of the experiments and analyzed data. JRK assisted with microarray and RNA sequencing analysis. GAE, RYY, and SL assisted with the generation and analysis of transplanted chimeras. KT provided statistical analyses. JZ and DCL wrote the paper.

Acknowledgments

Address correspondence to: Daniel C. Link, Division of Oncology, Department of Medicine, 660 South Euclid Avenue, Campus Box 8007, St. Louis, Missouri 63110, USA. Phone: 314.362.8871; Email: danielclink@wustl.edu.

1. Ding L, Saunders TL, Enikolopov G, Morrison SJ. Endothelial and perivascular cells maintain haematopoietic stem cells. *Nature*. 2012;481(7382):457–462.
2. Kunisaki Y, et al. Arteriolar niches maintain haematopoietic stem cell quiescence. *Nature*. 2013;502(7473):637–643.
3. Acar M, et al. Deep imaging of bone marrow shows non-dividing stem cells are mainly perisinusoidal. *Nature*. 2015;526(7571):126–130.
4. Chen JY, et al. Hoxb5 marks long-term haematopoietic stem cells and reveals a homogenous perivascular niche. *Nature*. 2016;530(7589):223–227.
5. Lévesque JP, Hendy J, Takamatsu Y, Simmons PJ, Bendall LJ. Disruption of the CXCR4/CXCL12 chemotactic interaction during hematopoietic stem cell mobilization induced by GCSF or cyclophosphamide. *J Clin Invest*. 2003;111(2):187–196.
6. Petit I, et al. G-CSF induces stem cell mobilization by decreasing bone marrow SDF-1 and up-regulating CXCR4. *Nat Immunol*. 2002;3(7):687–694.
7. Semerad CL, et al. G-CSF potently inhibits osteoblast activity and CXCL12 mRNA expression in the bone marrow. *Blood*. 2005;106(9):3020–3027.
8. Christopher MJ, Rao M, Liu F, Woloszynek JR, Link DC. Expression of the G-CSF receptor in monocytic cells is sufficient to mediate hematopoietic progenitor mobilization by G-CSF in mice. *J Exp Med*. 2011;208(2):251–260.
9. Chow A, et al. Bone marrow CD169+ macrophages promote the retention of hematopoietic stem and progenitor cells in the mesenchymal stem cell niche. *J Exp Med*. 2011;208(2):261–271.
10. Winkler IG, et al. Bone marrow macrophages maintain hematopoietic stem cell (HSC) niches and their depletion mobilizes HSCs. *Blood*. 2010;116(23):4815–4828.
11. Merad M, Sathe P, Helft J, Miller J, Mortha A. The dendritic cell lineage: ontogeny and function of dendritic cells and their subsets in the steady state and the inflamed setting. *Annu Rev Immunol*. 2013;31:563–604.
12. Jaitin DA, et al. Massively parallel single-cell RNA-seq for marker-free decomposition of tissues into cell types. *Science*. 2014;343(6172):776–779.
13. Sapoznikov A, Pewzner-Jung Y, Kalchenko V, Krauthgamer R, Shachar I, Jung S. Perivascular clusters of dendritic cells provide critical survival signals to B cells in bone marrow niches. *Nat Immunol*. 2008;9(4):388–395.
14. Cavanagh LL, et al. Activation of bone marrow-resident memory T cells by circulating, antigen-bearing dendritic cells. *Nat Immunol*. 2005;6(10):1029–1037.
15. Jung S, et al. Analysis of fractalkine receptor CX(3)CR1 function by targeted deletion and green fluorescent protein reporter gene insertion. *Mol Cell Biol*. 2000;20(11):4106–4114.
16. Evrard M, et al. Visualization of bone marrow monocyte mobilization using Cx3cr1gfp/+ Flt3L-/- reporter mouse by multiphoton intravital microscopy. *J Leukoc Biol*. 2015;97(3):611–619.
17. Pillai MM, Hayes B, Torok-Storb B. Inducible transgenes under the control of the hCD68 promoter identifies mouse macrophages with a distribution that differs from the F4/80 - and CSF-1R-expressing populations. *Exp Hematol*. 2009;37(12):1387–1392.
18. Reizis B. Classical dendritic cells as a unique immune cell lineage. *J Exp Med*. 2012;209(6):1053–1056.
19. Steinman RM. Decisions about dendritic cells: past, present, and future. *Annu Rev Immunol*. 2012;30:1–22.
20. Collin M, Bigley V. Human dendritic cell subsets: an update. *Immunology*. 2018;154(1):3–20.
21. Ginhoux F, et al. The origin and development of nonlymphoid tissue CD103+ DCs. *J Exp Med*. 2009;206(13):3115–3130.
22. See P, et al. Mapping the human DC lineage through the integration of high-dimensional techniques. *Science*. 2017;356(6342):eaag3009.
23. Meredith MM, et al. Expression of the zinc finger transcription factor zDC (Zbtb46, Btbd4) defines the classical dendritic cell lineage. *J Exp Med*. 2012;209(6):1153–1165.
24. Satpathy AT, et al. Zbtb46 expression distinguishes classical dendritic cells and their committed progenitors from other immune lineages. *J Exp Med*. 2012;209(6):1135–1152.
25. Liu Y, Pop R, Sadegh C, Brugnara C, Haase VH, Socolovsky M. Suppression of Fas-FasL coexpression by erythropoietin mediates erythroblast expansion during the erythropoietic stress response in vivo. *Blood*. 2006;108(1):123–133.
26. Kim TS, Hanak M, Trampont PC, Braciale TJ. Stress-associated erythropoiesis initiation is regulated by type 1 conventional dendritic cells.

J Clin Invest. 2015;125(10):3965–3980.

27. Lévesque JP, et al. Hematopoietic progenitor cell mobilization results in hypoxia with increased hypoxia-inducible transcription factor-1 alpha and vascular endothelial growth factor A in bone marrow. *Stem Cells*. 2007;25(8):1954–1965.

28. Itkin T, et al. Distinct bone marrow blood vessels differentially regulate haematopoiesis. *Nature*. 2016;532(7599):323–328.

29. Hoggatt J, et al. Rapid mobilization reveals a highly engraftable hematopoietic stem cell. *Cell*. 2018;172(1-2):191–204.e10.

30. Petri B, et al. Endothelial LSP1 is involved in endothelial dome formation, minimizing vascular permeability changes during neutrophil transmigration in vivo. *Blood*. 2011;117(3):942–952.

31. Köhler A, et al. G-CSF-mediated thrombopoietin release triggers neutrophil motility and mobilization from bone marrow via induction of Cxcr2 ligands. *Blood*. 2011;117(16):4349–4357.

32. Reutershan J, et al. Critical role of endothelial CXCR2 in LPS-induced neutrophil migration into the lung. *J Clin Invest*. 2006;116(3):695–702.

33. Lei X, Hossain M, Qadri SM, Liu L. Different microvascular permeability responses elicited by the CXC chemokines MIP-2 and KC during leukocyte recruitment: role of LSP1. *Biochem Biophys Res Commun*. 2012;423(3):484–489.

34. Villani AC, et al. Single-cell RNA-seq reveals new types of human blood dendritic cells, monocytes, and progenitors. *Science*. 2017;356(6335):eaah4573.

35. Schlitzer A, et al. Identification of cDC1- and cDC2-committed DC progenitors reveals early lineage priming at the common DC progenitor stage in the bone marrow. *Nat Immunol*. 2015;16(7):718–728.

36. Guilliams M, et al. Unsupervised high-dimensional analysis aligns dendritic cells across tissues and species. *Immunity*. 2016;45(3):669–684.

37. Pelus LM, Fukuda S. Peripheral blood stem cell mobilization: the CXCR2 ligand GRObeta rapidly mobilizes hematopoietic stem cells with enhanced engraftment properties. *Exp Hematol*. 2006;34(8):1010–1020.

38. Salvi V, et al. Dendritic cell-derived VEGF-A plays a role in inflammatory angiogenesis of human secondary lymphoid organs and is driven by the coordinated activation of multiple transcription factors. *Oncotarget*. 2016;7(26):39256–39269.

39. Webster B, Ekland EH, Agle LM, Chyou S, Ruggieri R, Lu TT. Regulation of lymph node vascular growth by dendritic cells. *J Exp Med*. 2006;203(8):1903–1913.

40. He H, et al. Perivascular macrophages limit permeability. *Arterioscler Thromb Vasc Biol*. 2016;36(11):2203–2212.

41. Karpova D, et al. Targeting VLA4 integrin and CXCR2 mobilizes serially repopulating hematopoietic stem cells. *J Clin Invest*. 2019;127(7):2745–2759.

42. Strasly M, et al. CCL16 activates an angiogenic program in vascular endothelial cells. *Blood*. 2004;103(1):40–49.

43. Hwang J, et al. Human CC chemokine CCL23, a ligand for CCR1, induces endothelial cell migration and promotes angiogenesis. *Cytokine*. 2005;30(5):254–263.

44. Dzenko KA, Song L, Ge S, Kuziel WA, Pachter JS. CCR2 expression by brain microvascular endothelial cells is critical for macrophage transendothelial migration in response to CCL2. *Microvasc Res*. 2005;70(1-2):53–64.

45. Saito M, et al. Diphtheria toxin receptor-mediated conditional and targeted cell ablation in transgenic mice. *Nat Biotechnol*. 2001;19(8):746–750.

46. Miyake Y, Asano K, Kaise H, Uemura M, Nakayama M, Tanaka M. Critical role of macrophages in the marginal zone in the suppression of immune responses to apoptotic cell-associated antigens. *J Clin Invest*. 2007;117(8):2268–2278.

47. Richards MK, Liu F, Iwasaki H, Akashi K, Link DC. Pivotal role of granulocyte colony-stimulating factor in the development of progenitors in the common myeloid pathway. *Blood*. 2003;102(10):3562–3568.

48. Zhang J, Link DC. Targeting of mesenchymal stromal cells by Cre-recombinase transgenes commonly used to target osteoblast lineage cells. *J Bone Miner Res*. 2016;31(11):2001–2007.

49. Durai V, Bagadia P, Briseño CG, Theisen DJ, et al. Altered compensatory cytokine signaling underlies the discrepancy between *Flt3*−/− and *Flt3l*−/− mice. *J Exp Med*. 2018;215(5):1417–1435.